European Journal of Mechanics B/Fluids 32 (2012) 22–31

Contents lists available at SciVerse ScienceDirect

European Journal of Mechanics B/Fluids

journal homepage: www.elsevier.com/locate/ejmflu

Hamiltonian higher-order nonlinear Schrödinger equations for broader-banded waves on deep water

Walter Craig [a], Philippe Guyenne [b,*], Catherine Sulem [c]

[a] Department of Mathematics, McMaster University, Hamilton, ON L8S 4K1, Canada
[b] Department of Mathematical Sciences, University of Delaware, Newark, DE 19716-2553, USA
[c] Department of Mathematics, University of Toronto, Toronto, ON M5S 2E4, Canada

ARTICLE INFO

Article history:
Received 10 January 2011
Received in revised form
4 June 2011
Accepted 22 September 2011
Available online 1 October 2011

Keywords:
Water waves
Nonlinear Schrödinger equation
Hamiltonian systems
Modulation theory
Dirichlet–Neumann operator
Symplectic integrators

ABSTRACT

Starting from the Hamiltonian formulation of the water wave problem and using the approach recently developed by Craig et al. (2010) [8], we derive Hamiltonian versions of the higher-order nonlinear Schrödinger equations for broader-banded deep-water waves, originally proposed by Trulsen and co-workers (1996, 2000) [4,5]. A Benjamin–Feir stability analysis is performed and shown to be in good agreement with previous work. Numerical simulations using a symplectic time integration scheme are also presented to illustrate the performance of these new models with regards to their conservative and Benjamin–Feir stability properties.

1. Introduction

The nonlinear Schrödinger (NLS) equation is a canonical model for describing the weakly nonlinear modulation of a train of surface gravity waves. It is accurate up to $O(\varepsilon^3)$ and is valid for waves of bandwidth $O(\varepsilon)$, where ε is a small parameter measuring the wave steepness. Besides inherent limitations related to the assumption of small wave steepness, the NLS equation also exhibits an unbounded region of Benjamin–Feir instability, in the case of two-dimensional sideband perturbations, which extends outside the regime of a narrow-banded spectrum. As a result, energy initially contained at low wavenumbers can leak to higher ones, as shown in numerical simulations of Martin and Yuen [1].

These limitations have prompted a number of initiatives in order to extend the range of applicability of the NLS equation. For deep-water waves, Dysthe [2] considered terms of up to $O(\varepsilon^4)$ (see [3] for the finite-depth case). His analysis reveals contributions from the mean flow induced by radiation stresses of the modulated wavetrain. This mean flow causes a local Doppler shift in the main direction of wave propagation, which results in improved stability properties. Subsequently, motivated by the fact that ocean wave spectra are usually not as narrow banded as assumed by the NLS equation, Trulsen and Dysthe [4] derived a high-order model similar to Dysthe's, which allows for waves of slightly larger bandwidth, $O(\varepsilon^{1/2})$. Their model essentially retains the same accuracy in nonlinearity as Dysthe's equation, but exhibits additional higher-order linear dispersive terms. Trulsen et al. [5] then took this idea further by combining the exact linear dispersion relation for deep-water waves with the cubic nonlinear terms of Dysthe's equation. This approach allows the exact linear dispersive term to be efficiently computed by a pseudo-spectral method, while retaining the relative simplicity of Dysthe's equation. A significant improvement on stability properties was observed in comparison with McLean's results on exact Stokes waves [6]. More specifically, Trulsen et al.'s analysis [5] reveals a bounded Benjamin–Feir instability region which prevents energy from leaking to high wavenumbers in their model.

While these earlier higher-order versions of the NLS equation have been applied with reasonable success to modeling a variety of wave phenomena, including four-wave interactions in applications to ocean wave spectra and rogue waves, they share a fundamental shortcoming: they are not Hamiltonian partial differential equations, despite the fact that they represent approximations to the Euler equations which can be written as a Hamiltonian system [7]. This in part motivated the recent work of

* Corresponding author. Tel.: +1 302 831 8664; fax: +1 302 831 4511.
E-mail address: guyenne@math.udel.edu (P. Guyenne).

0997-7546/$ – see front matter © 2011 Elsevier Masson SAS. All rights reserved.
doi:10.1016/j.euromechflu.2011.09.008

Craig et al. [8,9] who proposed a systematic Hamiltonian approach to nonlinear wave modulation. In particular, these authors derived Hamiltonian versions of Dysthe's equation for gravity water waves on both finite and infinite depth. The present paper takes this idea further by proposing Hamiltonian counterparts to the models derived by Trulsen and coworkers [4,5], using the method recently developed by Craig et al. [8]. These new Hamiltonian models, not only possess a high degree of accuracy, but are also consistent with the Hamiltonian formulation of the full water wave problem[1]. In addition to presenting their derivation, we also analyze their properties with regards to the Benjamin–Feir stability of a uniform wavetrain (i.e. a Stokes wave). These stability results are tested against numerical simulations using a fourth-order symplectic scheme for time integration. To our knowledge, this is the first time that results are reported on applications of this type of symplectic integrators to Hamiltonian higher-order NLS equations for water waves.

The remainder of the paper is organized as follows. In Section 2, we present the mathematical formulation of the problem including the Hamiltonian formulation of the equations of motion. Sections 3 and 4 describe the main steps in our Hamiltonian perturbation method, and Sections 5 and 6 give the derivation of our Hamiltonian models. The Benjamin–Feir stability analysis of these models is presented in Section 7, and numerical results are then discussed in Section 8. Finally, concluding remarks are given in Section 9.

2. Hamiltonian formulation and Dirichlet–Neumann operator

We consider the evolution of a free surface $\{y = \eta(x, t)\}$ on top of an infinitely deep fluid

$$S(\eta) = \{(x, y) \in \mathbb{R}^{n-1} \times \mathbb{R} : -\infty < y < \eta(x, t)\},$$

under the influence of gravity. Here, (x, y) denote the horizontal and vertical coordinates respectively, t is time, and $n = 2$ or 3 is the space dimension. The fluid is assumed to be incompressible, inviscid and the flow is irrotational, so that the free-surface elevation $\eta(x, t)$ and the velocity potential $\varphi(x, y, t)$ satisfy the boundary value problem

$$\nabla^2\varphi = 0 \quad \text{in } S(\eta), \tag{1}$$

$$\partial_t\eta + \partial_x\eta \cdot \partial_x\varphi - \partial_y\varphi = 0 \quad \text{at } y = \eta(x, t), \tag{2}$$

$$\partial_t\varphi + \frac{1}{2}|\nabla\varphi|^2 + g\eta = 0 \quad \text{at } y = \eta(x, t), \tag{3}$$

$$\partial_y\varphi \to 0 \quad \text{as } y \to -\infty, \tag{4}$$

where g denotes the acceleration due to gravity and $\nabla = (\partial_x, \partial_y)^\top$.

Following Craig and Sulem [12], we can reduce the dimensionality of the classical formulation (1)–(4) for the water wave problem by considering surface quantities as unknowns. This can be accomplished by introducing the Dirichlet–Neumann operator (DNO)

$$G(\eta)\xi = (-\partial_x\eta, 1)^\top \cdot \nabla\varphi|_{y=\eta}, \tag{5}$$

which takes Dirichlet data $\xi(x, t) = \varphi(x, \eta(x, t), t)$ at the free surface, solves the Laplace equation (1) for φ with boundary condition (4), and returns the corresponding Neumann data (i.e. the normal fluid velocity at the free surface).

[1] After we submitted this paper, we learnt about the recent work of Gramstad and Trulsen [10] who derived a Hamiltonian form of the modified NLS equation for gravity waves on arbitrary depth, starting from Krasitskii's version [11] of Zakharov's equation.

In terms of ξ and $G(\eta)\xi$, Eqs. (1)–(4) reduce to

$$\partial_t\eta = G(\eta)\xi, \tag{6}$$

$$\begin{aligned}\partial_t\xi \;=\; & -g\eta - \frac{1}{2(1 + |\partial_x\eta|^2)} \\ & \times [|\partial_x\xi|^2 - (G(\eta)\xi)^2 - 2(\partial_x\xi \cdot \partial_x\eta)G(\eta)\xi \\ & + |\partial_x\xi|^2|\partial_x\eta|^2 - (\partial_x\xi \cdot \partial_x\eta)^2],\end{aligned} \tag{7}$$

which are Hamiltonian equations in Zakharov's formulation of the water wave problem [7,12,13]. These can be expressed in the canonical form

$$\partial_t \begin{pmatrix}\eta \\ \xi\end{pmatrix} = \begin{pmatrix}0 & 1 \\ -1 & 0\end{pmatrix}\begin{pmatrix}\delta_\eta H \\ \delta_\xi H\end{pmatrix}, \tag{8}$$

for the conjugate variables η and ξ, with the Hamiltonian

$$H = \frac{1}{2}\int [\xi G(\eta)\xi + g\eta^2]dx. \tag{9}$$

Eq. (9) can be thought of as the total energy of the system, with the first and second terms representing the kinetic and potential energies respectively.

It has been shown that the DNO is an analytic function of η provided the free surface is sufficiently regular [14], which implies that the DNO can be written in terms of a convergent Taylor series expansion

$$G(\eta) = \sum_{j=0}^{\infty} G_j(\eta), \tag{10}$$

where the Taylor polynomials G_j can be determined recursively [12]. However, only contributions of up to second order in η, i.e.

$$G_0 = |D_x|,$$

$$G_1 = D_x\eta \cdot D_x - G_0\eta G_0,$$

$$G_2 = -\frac{1}{2}(|D_x|^2\eta^2 G_0 + G_0\eta^2|D_x|^2 - 2G_0\eta G_0\eta G_0),$$

are needed for the purposes of the present study, as they include all the contributions relevant to four-wave interactions [15]. Note that $D_x = -i\partial_x$ (so its Fourier symbol is k) and, in the case of a (constant) finite depth h, the only modification to this formulation is $G_0 = |D_x|\tanh(h|D_x|)$ [12,13]. The reader may refer to [16–21,13] for applications of this formulation to long-wave perturbation calculations as well as direct numerical simulations of nonlinear waves on both uniform and variable depth.

3. Canonical transformations and modulational Ansatz

Following Craig et al. [22,8,9,23], our Hamiltonian approach for deriving envelope models involves canonical transformations that approximate the original Hamiltonian of the system and change the corresponding symplectic structure. First, we introduce the normal modes $(z, \bar{z}, \widetilde{\eta}, \widetilde{\xi})$ defined by

$$\eta = \frac{1}{\sqrt{2}}a^{-1}(D_x)(z + \bar{z}) + \widetilde{\eta}, \quad \widetilde{\eta} = P_0\eta, \tag{11}$$

$$\xi = \frac{1}{\sqrt{2}i}a(D_x)(z - \bar{z}) + \widetilde{\xi}, \quad \widetilde{\xi} = P_0\xi, \tag{12}$$

where

$$a(D_x) = \sqrt[4]{\frac{g}{G_0}},$$

and $(\widetilde{\eta}, \widetilde{\xi})$ are the zeroth modes representing the mean flow. The symbol $\bar{\cdot}$ stands for complex conjugation, and P_0 is the projection

that associates to (η, ξ) their zeroth-frequency components. We split the zeroth modes from the higher ones in this decomposition because otherwise $a^{-1}(0) = 0$ and so the transformation $(\eta, \xi) \to (z, \bar{z})$ is singular for $k = 0$. As a result, system (8) becomes

$$\partial_t \begin{pmatrix} z \\ \bar{z} \\ \widetilde{\eta} \\ \widetilde{\xi} \end{pmatrix} = \begin{pmatrix} 0 & -i(\mathbb{I} - P_0) & 0 & 0 \\ i(\mathbb{I} - P_0) & 0 & 0 & 0 \\ 0 & 0 & 0 & P_0 \\ 0 & 0 & -P_0 & 0 \end{pmatrix} \begin{pmatrix} \delta_z H \\ \delta_{\bar{z}} H \\ \delta_{\widetilde{\eta}} H \\ \delta_{\widetilde{\xi}} H \end{pmatrix}, \tag{13}$$

where $\mathbb{I}$ is the identity operator.

The next step is to introduce the modulational Ansatz

$$z = \varepsilon u(X, t) e^{ik_0 \cdot x}, \qquad \bar{z} = \varepsilon \bar{u}(X, t) e^{-ik_0 \cdot x}, \tag{14}$$

$$\widetilde{\eta} = \varepsilon^{\alpha + 1/2} \widetilde{\eta}_1(X, t), \qquad \widetilde{\xi} = \varepsilon^{\alpha} \widetilde{\xi}_1(X, t), \tag{15}$$

which is to say that we look for solutions in the form of monochromatic waves with carrier wavenumber $k_0 \in \mathbb{R}^{n-1}_+ \setminus \{0\}$ and with slowly varying complex envelope u depending on $X = \varepsilon^{1/2} x$. As suggested by Trulsen and Dysthe [4], this choice of long spatial scale allows for waves of slightly larger bandwidth than assumed by the NLS and Dysthe equations. The exponent $\alpha \geq 1$ is to be determined by the subsequent asymptotic procedure, and $\varepsilon = O(|k_0| a_0) \ll 1$ is a small parameter measuring the wave steepness (a_0 is a typical wave amplitude). In (15), there is a difference by an exponent $1/2$ in the power of ε between the mean fields $\widetilde{\eta}$ and $\widetilde{\xi}$ because we anticipate that $\widetilde{\eta} \sim \partial_x \widetilde{\xi}$ similarly to the long-wave regime [17,22,19]. The corresponding equations of motion are given by

$$\partial_t \begin{pmatrix} u \\ \bar{u} \\ \widetilde{\eta}_1 \\ \widetilde{\xi}_1 \end{pmatrix} = \begin{pmatrix} 0 & -i\varepsilon^{(n-5)/2} \mathbb{I}' & 0 & 0 \\ i\varepsilon^{(n-5)/2} \mathbb{I}' & 0 & 0 & 0 \\ 0 & 0 & 0 & \varepsilon^{(n-2-4\alpha)/2} \\ 0 & 0 & -\varepsilon^{(n-2-4\alpha)/2} & 0 \end{pmatrix} \times \begin{pmatrix} \delta_u H \\ \delta_{\bar{u}} H \\ \delta_{\widetilde{\eta}_1} H \\ \delta_{\widetilde{\xi}_1} H \end{pmatrix}, \tag{16}$$

where $\mathbb{I}'$ is the identity on the class of functions $\{u(X)\}$, and the final 2×2 block retains essentially the standard symplectic form on the two-dimensional space of functions $(\widetilde{\eta}_1, \widetilde{\xi}_1)$.

Note the successive changes in the symplectic structure of the system, as represented by the different coefficient matrices on the right-hand side of (8), (13) and (16). Further details on these canonical transformations can be found in [22,8].

4. Expansion and reduction of the Hamiltonian

The expression of the Hamiltonian (9) is also transformed through the changes of variables (11)–(12) and (14)–(15). The first transformation diagonalizes the quadratic (i.e. linear) part of the Hamiltonian, so as to exhibit more clearly the natural frequencies of the system. The second one introduces the small parameter ε and, together with the Taylor series expansion of the DNO, this allows us to expand H in powers of ε. For example, the Fourier multiplier $D_x = \varepsilon^{1/2} D_X$ when acting on functions of X only, while $D_x = \pm k_0 + \varepsilon^{1/2} D_X$ when acting on functions of the form $u(X) e^{\pm i k_0 \cdot x}$ [23].

Moreover, since we look for solutions in the form of multiple scale functions, with the slowly varying components being the focus of our attention, further simplifications can be achieved by only retaining resonant terms in the Hamiltonian. This homogenization (or averaging) procedure is based on the scale separation result of Craig et al. [19], which implies that terms with fast oscillations essentially homogenize to zero and thus do not contribute to the effective Hamiltonian. More specifically, if $g(x)$ is a periodic function and $f(X)$ is a Schwartz class function, then

$$\int g\left(\frac{X}{\sqrt{\varepsilon}}\right) f(X) dX = E(g) \int f(X) dX + O(\varepsilon^N),$$

for any $N > 0$, with $E(g)$ being the average value of g over a fundamental domain. A more precise statement of this result together with its proof can be found in [19]. In the present setting, the homogenized coefficients are of the form

$$E(g) = E(e^{ik_0 n \cdot x}) = \begin{cases} 1 & \text{if } n = 0, \\ 0 & \text{if } n \neq 0, \end{cases}$$

which may be interpreted as resonance conditions for n-wave interactions.

Starting from the decomposition

$$H = H_2 + H_3 + H_4 + \cdots,$$

where

$$H_2 = \frac{1}{2} \int (\xi G_0 \xi + g \eta^2) dx, \qquad H_3 = \frac{1}{2} \int \xi G_1 \xi dx,$$

$$H_4 = \frac{1}{2} \int \xi G_2 \xi dx,$$

we obtain, after transformations and simplifications,

$$H_2 = \varepsilon^{(5-n)/2} \int \left[\bar{u}\, \omega(k_0 + \varepsilon^{1/2} D_X) u + \frac{1}{2} \varepsilon^{2\alpha - 3/2} \widetilde{\xi}_1 |D_X| \widetilde{\xi}_1 + \frac{g}{2} \varepsilon^{2\alpha - 1} \widetilde{\eta}_1^2 \right] dX + \cdots, \tag{17}$$

$$H_3 = \frac{i}{2} \varepsilon^{(6 + 2\alpha - n)/2} \int \left\{ [2k_0 |u|^2 + \varepsilon^{1/2} (\bar{u} D_X u + u \overline{D_X u})] \cdot D_X \widetilde{\xi}_1 + \frac{1}{2} \varepsilon^{1/2} \frac{k_0}{|k_0|} \cdot (\bar{u} D_X u - u \overline{D_X u}) |D_X| \widetilde{\xi}_1 \right\} dX + \cdots, \tag{18}$$

$$H_4 = \frac{1}{4} \varepsilon^{(9-n)/2} |k_0|^3 \int \left[|u|^4 + \frac{3}{2} \varepsilon^{1/2} \frac{k_0}{|k_0|^2} \cdot |u|^2 (\bar{u} D_X u + u \overline{D_X u}) \right] dX + \cdots, \tag{19}$$

where $\omega(D_x) = (gG_0)^{1/2} = (g|D_x|)^{1/2}$ is the Fourier multiplier representing the exact linear dispersion relation of the problem.

5. $O(\varepsilon^{5/2})$ model

If we now expand $\omega(k_0 + \varepsilon^{1/2} D_X)$ up to $O(\varepsilon^{5/2})$ so as to consider the same order of approximation as in [4], and collect the various terms, we find

$$\begin{aligned} H = {} & \varepsilon^{(5-n)/2} \int \frac{\bar{u}}{2} \left[\omega(k_0) + \varepsilon^{1/2} \partial_k \omega(k_0) \cdot D_X \right. \\ & \left. + \frac{\varepsilon}{2} \partial^2_{k_j k_l} \omega(k_0) D^2_{X_j X_l} + \cdots + \frac{\varepsilon^{5/2}}{120} \partial^5 \omega(k_0) D^5 \right] u \\ & + \text{c.c.} + \frac{1}{2} \varepsilon^{2\alpha - 3/2} \widetilde{\xi}_1 |D_X| \widetilde{\xi}_1 + \frac{g}{2} \varepsilon^{2\alpha - 1} \widetilde{\eta}_1^2 \\ & + \frac{i}{2} \varepsilon^{\alpha + 1/2} [2k_0 |u|^2 + \varepsilon^{1/2} (\bar{u} D_X u + u \overline{D_X u})] \cdot D_X \widetilde{\xi}_1 \\ & + \frac{i}{4} \varepsilon^{\alpha + 1} \frac{k_0}{|k_0|} \cdot (\bar{u} D_X u - u \overline{D_X u}) |D_X| \widetilde{\xi}_1 \\ & + \frac{\varepsilon^2}{4} |k_0|^3 \left[|u|^4 + \frac{3}{2} \varepsilon^{1/2} \frac{k_0}{|k_0|^2} \cdot |u|^2 (\bar{u} D_X u + u \overline{D_X u}) \right] dX \\ & + \ldots, \end{aligned} \tag{20}$$

where 'c.c.' stands for the complex conjugate of all the preceding terms on the right-hand side of the equation. Dominant balance suggests that $2\alpha - 3/2 = 5/2$ and thus $\alpha = 2$, which leads to

$$\begin{aligned}\varepsilon^{(n-5)/2}H = \int \frac{\overline{u}}{2}\Bigg[&\omega(k_0) + \varepsilon^{1/2}\partial_k\omega(k_0)\cdot D_X \\ &+ \frac{\varepsilon}{2}\partial^2_{k_jk_l}\omega(k_0)D^2_{X_jX_l} + \cdots + \frac{\varepsilon^{5/2}}{120}\partial^5\omega(k_0)D^5\Bigg]u \\ &+ \text{c.c.} + \frac{\varepsilon^2}{4}|k_0|^3|u|^4 + \varepsilon^{5/2}\Bigg[\frac{1}{2}\widetilde{\xi}_1|D_X|\widetilde{\xi}_1 \\ &+ i|u|^2k_0\cdot D_X\widetilde{\xi}_1 + \frac{3}{8}|k_0|k_0\cdot|u|^2(\overline{u}D_Xu \\ &+ u\overline{D_Xu})\Bigg]dX + O(\varepsilon^3). \end{aligned} \tag{21}$$

In this equation, the Einstein summation convention is used for repeated indices ($j, l = \{1, \ldots, n-1\}$), and the fifth-order derivative term is expressed in the short multi-index notation. The so-obtained Hamiltonian can be further reduced by subtracting multiples of the conserved wave action

$$M = \varepsilon^{(5-n)/2}\int |u|^2dX, \tag{22}$$

and of the conserved impulse (or momentum)

$$\begin{aligned} I &= \int \eta\partial_x\xi\, dx, \\ &= \varepsilon^{(5-n)/2}\int\Bigg[k_0|u|^2 + \frac{\varepsilon^{1/2}}{2}(\overline{u}D_Xu + u\overline{D_Xu}) \\ &\quad + i\varepsilon^3\widetilde{\eta}_1D_X\widetilde{\xi}_1\Bigg]dX, \end{aligned} \tag{23}$$

so that the reduced form is

$$\begin{aligned}&\varepsilon^{(n-5)/2}\widehat{H} \\ &= \varepsilon^{(n-5)/2}\{H - \partial_k\omega(k_0)\cdot I - [\omega(k_0) - k_0\cdot\partial_k\omega(k_0)]M\}, \\ &= \frac{\varepsilon}{2}\int\Bigg\{\frac{\overline{u}}{2}\Bigg[\partial^2_{k_jk_l}\omega(k_0)D^2_{X_jX_l} + \cdots + \frac{\varepsilon^{3/2}}{60}\partial^5\omega(k_0)D^5\Bigg]u \\ &\quad + \text{c.c.} + \frac{\varepsilon}{2}|k_0|^3|u|^4 + \varepsilon^{3/2}\Bigg[\widetilde{\xi}_1|D_X|\widetilde{\xi}_1 + 2i|u|^2k_0\cdot D_X\widetilde{\xi}_1 \\ &\quad + \frac{3}{4}|k_0|k_0\cdot|u|^2(\overline{u}D_Xu + u\overline{D_Xu})\Bigg]\Bigg\}dX + O(\varepsilon^3). \end{aligned} \tag{24}$$

Introducing M is equivalent to saying that our approximation of the problem is phase invariant (as is typically the case for the NLS and Dysthe equations). Subtracting I from H is equivalent to changing the coordinate system into a reference frame moving with the group velocity $\partial_k\omega(k_0)$ [22,8].

From (16), the corresponding equations of motion read

$$\begin{aligned} 2i\partial_\tau u \;=\;& \partial^2_{k_jk_l}\omega(k_0)D^2_{X_jX_l}u + \cdots + \frac{\varepsilon^{3/2}}{60}\partial^5\omega(k_0)D^5u \\ &+ \varepsilon|k_0|^3|u|^2u + \varepsilon^{3/2}(2ik_0\cdot uD_X\widetilde{\xi}_1 + 3|k_0|k_0 \\ &\cdot|u|^2D_Xu) + O(\varepsilon^2), \end{aligned} \tag{25}$$

$$\varepsilon\partial_\tau\widetilde{\eta}_1 = |D_X|\widetilde{\xi}_1 - ik_0\cdot D_X|u|^2 + O(\varepsilon^{1/2}), \tag{26}$$

$$\varepsilon\partial_\tau\widetilde{\xi}_1 = O(\varepsilon^{1/2}), \tag{27}$$

where $\tau = \varepsilon t$ is a slow time. Noting that the mean field $\widetilde{\xi}_1$ only appears at order $O(\varepsilon^{3/2})$ in (25), we can solve (26) for $\widetilde{\xi}_1$ at leading order,

$$\widetilde{\xi}_1 = i|D_X|^{-1}k_0\cdot D_X|u|^2 + O(\varepsilon^{1/2}), \tag{28}$$

and plug this expression in (25). The resulting closed equation for the complex envelope u,

$$\begin{aligned} 2i\partial_\tau u \;=\;& -\partial^2_{k_jk_l}\omega(k_0)\partial^2_{X_jX_l}u + \cdots - i\frac{\varepsilon^{3/2}}{60}\partial^5\omega(k_0)\partial^5u \\ &+ \varepsilon|k_0|^3|u|^2u + \varepsilon^{3/2}(2uk_{0j}k_{0l}|D_X|^{-1}\partial^2_{X_jX_l}|u|^2 \\ &- 3i|k_0|k_0\cdot|u|^2\partial_Xu), \end{aligned} \tag{29}$$

is a Hamiltonian version of the model derived by Trulsen and Dysthe [4]. It can be cast into the symplectic form

$$\partial_\tau u = -i\delta_{\overline{u}}H, \tag{30}$$

with the Hamiltonian

$$\begin{aligned} H \;=\;& \frac{1}{2}\int\Bigg\{\frac{\overline{u}}{2}\Bigg[-\partial^2_{k_jk_l}\omega(k_0)\partial^2_{X_jX_l} + \cdots - i\frac{\varepsilon^{3/2}}{60}\partial^5\omega(k_0)\partial^5\Bigg]u \\ &+ \text{c.c.} + \frac{\varepsilon}{2}|k_0|^3|u|^4 + \varepsilon^{3/2}\Bigg[\frac{3}{2}|k_0|k_0\cdot|u|^2\Im(\overline{u}\partial_Xu) \\ &- k_{0j}k_{0l}(\partial_{X_j}|u|^2)|D_X|^{-1}\partial_{X_l}|u|^2\Bigg]\Bigg\}dX, \end{aligned} \tag{31}$$

where $\Im$ denotes the imaginary part. This closed-form Hamiltonian results from (24) by substituting $\widetilde{\xi}_1$ with (28).

We remark that, in the finite-depth case, dominant balance would likely imply a smaller value of α, which means that the mean flow would occur at a lower order in the asymptotic analysis. Derivations in this case for waves of bandwidth $O(\varepsilon)$ can be found in [8].

6. $O(\varepsilon^{5/2})$ model with exact linear dispersion

As suggested by Trulsen et al. [5], a better approximation can be achieved by expanding the nonlinear terms in (9) up to $O(\varepsilon^{5/2})$ as previously, while keeping the linear dispersion relation exact. In the present framework, the resulting envelope equation is

$$\begin{aligned} 2i\partial_\tau u \;=\;& \frac{2}{\varepsilon}[\omega(k_0 + \varepsilon^{1/2}D_X) - \omega(k_0)]u + \varepsilon|k_0|^3|u|^2u \\ &+ \varepsilon^{3/2}(2uk_{0j}k_{0l}|D_X|^{-1}\partial^2_{X_jX_l}|u|^2 \\ &- 3i|k_0|k_0\cdot|u|^2\partial_Xu), \end{aligned} \tag{32}$$

which can be viewed as a Hamiltonian version of the model derived in [5], and the corresponding Hamiltonian is given by

$$\begin{aligned} H \;=\;& \frac{1}{2}\int\Bigg\{\frac{2}{\varepsilon}\overline{u}[\omega(k_0 + \varepsilon^{1/2}D_X) - \omega(k_0)]u + \frac{\varepsilon}{2}|k_0|^3|u|^4 \\ &+ \varepsilon^{3/2}\Bigg[\frac{3}{2}|k_0|k_0\cdot|u|^2\Im(\overline{u}\partial_Xu) \\ &- k_{0j}k_{0l}(\partial_{X_j}|u|^2)|D_X|^{-1}\partial_{X_l}|u|^2\Bigg]\Bigg\}dX. \end{aligned} \tag{33}$$

Note that the extra term proportional to $\omega(k_0)$ in (33) is due to the reduction $H \to H - \omega(k_0)M$, and the symplectic structure (30) still holds true for this case.

Eq. (32) looks very similar to that derived by Trulsen et al. [5] in its general form, with the exception that a higher-order nonlinear term like $k_0\cdot u^2\partial_X\overline{u}$ is absent, and here we are also able to explicitly close the equation by solving for the mean flow. The same observations apply to (29) in comparison with the model of Trulsen and Dysthe [4]. It is possible to recover the original models from their Hamiltonian counterparts by a change of variables, as shown in [8] for the Hamiltonian Dysthe equation, but this transformation is not canonical. Eq. (32) also closely resembles the Hamiltonian model of Gramstad and Trulsen [10] in its deep-water limit, although these authors did not express their equation in an explicitly closed form.

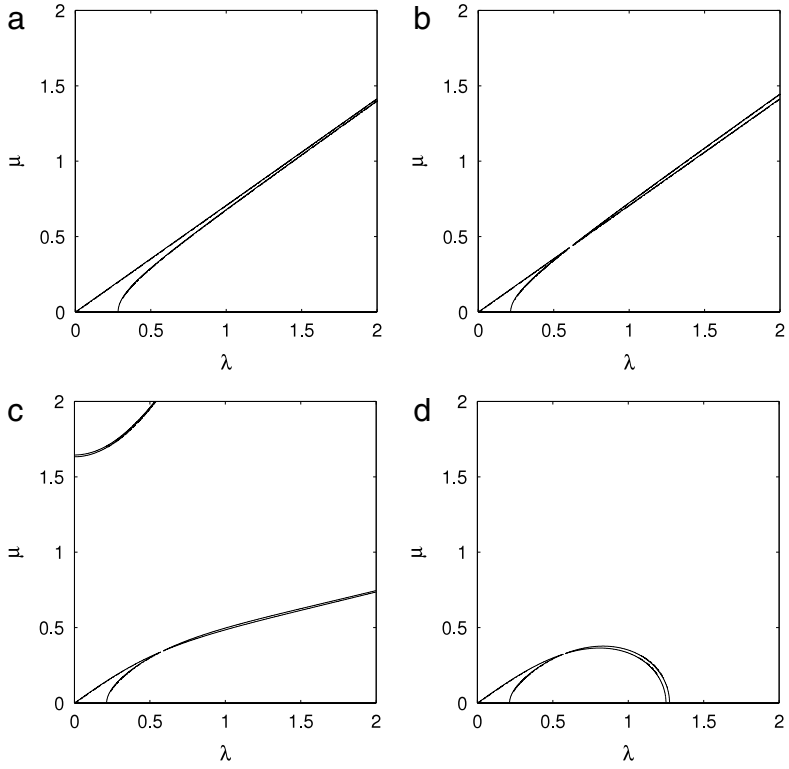

Fig. 1. Comparison of instability regions for $A_0 = 0.1$ and $\varepsilon = 1$ between (a) the NLS equation, (b) the Hamiltonian Dysthe equation, (c) model (29) and (d) model (32).

7. Stability of Stokes waves

Both models (29) and (32) admit uniform wavetrain solutions

$$u_0(\tau) = A_0 e^{-\frac{i}{2}\varepsilon k_0^3 A_0^2 \tau},$$

where A_0 is a real constant, which correspond to progressive Stokes waves. In this section, we analyze the modulational or Benjamin–Feir stability of these solutions, i.e. their linear stability with respect to sideband perturbations. For this purpose, we consider the general three-dimensional case $n = 3$ such that $x = (x_1, x_2)^\top \in \mathbb{R}^2$, and we assume that k_0 points in the x_1-direction.

Examining model (29) first, if we insert a perturbed solution of the form

$$u(X, \tau) = u_0(\tau)[1 + B(X, \tau)],$$

where

$$B(X, \tau) = B_1 e^{\Omega\tau + i(\lambda X_1 + \mu X_2)} + B_2 e^{\overline{\Omega}\tau - i(\lambda X_1 + \mu X_2)},$$

and B_1, B_2 are complex coefficients, we find that the condition $\Re(\Omega) \neq 0$ for instability yields

$$\begin{aligned} &\varepsilon A_0^2 \sqrt{g k_0} \left(\frac{\lambda^2}{2} - \mu^2 + \frac{15}{96}\varepsilon\frac{\lambda^4}{k_0^2} - \frac{15}{8}\varepsilon\frac{\lambda^2\mu^2}{k_0^2} + \frac{9}{24}\varepsilon\frac{\mu^4}{k_0^2} \right) \\ &\quad \times \left(k_0 - 2\varepsilon^{1/2}\frac{\lambda^2}{\sqrt{\lambda^2+\mu^2}} \right) \\ &\quad - \frac{g}{4k_0^3}\left(\frac{\lambda^2}{2} - \mu^2 + \frac{15}{96}\varepsilon\frac{\lambda^4}{k_0^2} - \frac{15}{8}\varepsilon\frac{\lambda^2\mu^2}{k_0^2} + \frac{9}{24}\varepsilon\frac{\mu^4}{k_0^2} \right)^2 \\ &> 0, \end{aligned} \tag{34}$$

where $\Re$ denotes the real part. This somewhat straightforward but tedious calculation is similar to those presented in [3,2,24,4,5], therefore we skip the details and only show the final result for the reader's convenience.

Applying the same strategy to model (32), we find that sideband instability occurs when

$$\begin{aligned} &2\varepsilon^2 k_0^2 A_0^2 [\mathcal{D}(\lambda, \mu) + \mathcal{D}(-\lambda, \mu)] \left(k_0 - 2\varepsilon^{1/2}\frac{\lambda^2}{\sqrt{\lambda^2+\mu^2}} \right) \\ &\quad - [\mathcal{D}(\lambda, \mu) + \mathcal{D}(-\lambda, \mu)]^2 > 0, \end{aligned} \tag{35}$$

which is expressed in terms of the exact linear multiplier

$$\mathcal{D}(\lambda, \mu) = \sqrt{g k_0} - \sqrt{g[(k_0 + \varepsilon^{1/2}\lambda)^2 + \varepsilon\mu^2]^{1/2}}.$$

As expected, both (34) and (35) indicate that the linear dispersive terms as well as the mean-flow term play an important role on the growth of sideband perturbations. In particular, we clearly notice the 'Doppler shift' relative to the carrier wavenumber k_0, due to the mean flow.

Fig. 1 shows the instability regions enclosed by the zero-level contour of conditions (34) and (35). As a reference, we also include the plots of the instability regions for the cubic NLS and Hamiltonian Dysthe equations as derived in [8]. To allow for direct comparison with existing results [6,4,5], we choose the parameter values $A_0 = 0.1$, $g = 1$, $k_0 = 1$ and $\varepsilon = 1$. The latter choice of value for ε allows for a more suitable scaling-independent inter-comparison between the different asymptotic models under consideration. Overall, we observe strong similarities with previously published results based on other Hamiltonian [10] and non-Hamiltonian models [5]. A clear improvement from (29) and (32) over the NLS and Dysthe equations is that the neutral stability curves are no longer straight lines. In particular, the instability region for (32) is localized near the origin and takes an arched shape connecting back to the λ-axis, which closely resembles McLean's class I results on exact Stokes waves of small amplitude [6]. This supports the idea that linear dispersion strongly affects the Benjamin–Feir instability process.

8. Numerical results

Although the analysis and derivations presented in the previous sections apply to the general three-dimensional case, for convenience here, we will only show two-dimensional ($n = 2$) numerical simulations. In this situation, models (29) and (32) simplify respectively into

$$\begin{aligned} 2i\partial_\tau u = & -\partial_k^2\omega(k_0)\partial_X^2 u + i\frac{\varepsilon^{1/2}}{3}\partial_k^3\omega(k_0)\partial_X^3 u \\ & + \frac{\varepsilon}{12}\partial_k^4\omega(k_0)\partial_X^4 u - i\frac{\varepsilon^{3/2}}{60}\partial_k^5\omega(k_0)\partial_X^5 u \\ & + \varepsilon k_0^3|u|^2 u - \varepsilon^{3/2}k_0^2(2u|D_X|\,|u|^2 + 3i|u|^2\partial_X u), \end{aligned} \tag{36}$$

whose Hamiltonian is

$$\begin{aligned} H = & \frac{1}{2}\int\left\{\frac{\overline{u}}{2}\left[-\partial_k^2\omega(k_0)\partial_X^2 + i\frac{\varepsilon^{1/2}}{3}\partial_k^3\omega(k_0)\partial_X^3\right.\right. \\ & + \left.\frac{\varepsilon}{12}\partial_k^4\omega(k_0)\partial_X^4 - i\frac{\varepsilon^{3/2}}{60}\partial_k^5\omega(k_0)\partial_X^5\right]u \\ & + \text{c.c.} + \frac{\varepsilon}{2}k_0^3|u|^4 + \varepsilon^{3/2}k_0^2\left[\frac{3}{2}|u|^2\Im(\overline{u}\partial_X u)\right. \\ & \left.\left. - \ |u|^2|D_X||u|^2\right]\right\}dX, \end{aligned} \tag{37}$$

and

$$\begin{aligned} 2i\partial_\tau u = & \frac{2}{\varepsilon}[\omega(k_0+\varepsilon^{1/2}D_X) - \omega(k_0)]u + \varepsilon k_0^3|u|^2 u \\ & - \varepsilon^{3/2}k_0^2(2u|D_X|\,|u|^2 + 3i|u|^2\partial_X u), \end{aligned} \tag{38}$$

with the Hamiltonian

$$\begin{aligned} H = & \frac{1}{2}\int\left\{\frac{2}{\varepsilon}\overline{u}[\omega(k_0+\varepsilon^{1/2}D_X) - \omega(k_0)]u + \frac{\varepsilon}{2}k_0^3|u|^4\right. \\ & \left. + \ \varepsilon^{3/2}k_0^2\left[\frac{3}{2}|u|^2\Im(\overline{u}\partial_X u) - |u|^2|D_X|\,|u|^2\right]\right\}dX. \end{aligned} \tag{39}$$

Note that now $X = X_1 \in \mathbb{R}$ and $k_0 > 0$.

The purpose of this section is twofold. First, we want to numerically check that models (29) and (32) derived in Sections 5 and 6 conserve their respective Hamiltonians in time. Second, we want to numerically test and validate the stability analysis presented in Section 7. Since this analysis only concerns linear stability while the problem is nonlinear, it is of interest to examine e.g. the validity of these results for long time intervals. Furthermore, we take this opportunity to introduce a symplectic numerical scheme for time integration of the two proposed models, motivated by the fact that they are Hamiltonian. We emphasize however that our intention is not to claim that this scheme is crucial for correctly simulating these Hamiltonian equations, nor is it superior to other (non-symplectic) schemes. This debate is beyond the scope of the present paper. Rather, we want to offer a possible choice of symplectic time integrator which is both numerically efficient and accurate. Details are given below.

8.1. Numerical methods

For space discretization, we use a pseudospectral method assuming periodic boundary conditions in X [12,21,25]. More specifically, the complex envelope u is approximated by a truncated Fourier series. Spatial derivatives and nonlocal Fourier multipliers are evaluated in Fourier space, while nonlinear products are calculated in physical space, on a grid of N equally spaced points. For example, the term $\omega(k_0+\varepsilon^{1/2}D_X)u$ in (38) can be efficiently computed by

$$\mathcal{F}^{-1}[\sqrt{g|k_0+\varepsilon^{1/2}\lambda|}\mathcal{F}(u)],$$

using the fast Fourier transform $\mathcal{F}$. Aliasing errors are removed by zero-padding in Fourier space, meaning that for the calculation of the nonlinear terms, the size of the solution's spectrum is extended by a factor of 2 and the extra modes are set to zero.

Time integration of (36) and (38) is performed in Fourier space, so that the linear terms can be solved exactly by the integrating factor technique. For illustration, let us consider model (38) in its Fourier form

$$\partial_\tau\widehat{u} = \mathcal{L}\widehat{u} + \mathcal{N}(\widehat{u}),$$

where

$$\mathcal{L} = -\frac{i}{\varepsilon}\left[\sqrt{g|k_0+\varepsilon^{1/2}\lambda|} - \sqrt{gk_0}\right],$$

is the Fourier multiplier of the linear part ($\overline{\mathcal{L}} = -\mathcal{L}$), $\mathcal{N}(\widehat{u})$ is the nonlinear part and $\widehat{u}(\lambda,\tau) = \mathcal{F}(u(X,\tau))$. Then making the change of variables

$$\widehat{u}(\lambda,\tau) = e^{\mathcal{L}\tau}\widehat{v}(\lambda,\tau), \tag{40}$$

leads to the following nonlinear evolution equation for $\widehat{v}$,

$$\partial_\tau\widehat{v} = e^{-\mathcal{L}\tau}\mathcal{N}(e^{\mathcal{L}\tau}\widehat{v}) = \widetilde{\mathcal{N}}(\widehat{v}). \tag{41}$$

Because Eq. (40) is a canonical transformation [22,8,13], through which

$$\partial_\tau\begin{pmatrix}\widehat{u}\\ \overline{\widehat{u}}\end{pmatrix} = \begin{pmatrix}0 & -i\mathbb{I}'\\ i\mathbb{I}' & 0\end{pmatrix}\begin{pmatrix}\delta_{\widehat{u}}H\\ \delta_{\overline{\widehat{u}}}H\end{pmatrix},$$

is transformed into

$$\begin{aligned} \partial_\tau\begin{pmatrix}\widehat{v}\\ \overline{\widehat{v}}\end{pmatrix} &= \begin{pmatrix}e^{-\mathcal{L}\tau} & 0\\ 0 & e^{\mathcal{L}\tau}\end{pmatrix}\begin{pmatrix}0 & -i\mathbb{I}'\\ i\mathbb{I}' & 0\end{pmatrix}\begin{pmatrix}e^{-\mathcal{L}\tau} & 0\\ 0 & e^{\mathcal{L}\tau}\end{pmatrix}^{\top}\begin{pmatrix}\delta_{\widehat{v}}H\\ \delta_{\overline{\widehat{v}}}H\end{pmatrix}, \\ &= \begin{pmatrix}0 & -i\mathbb{I}'\\ i\mathbb{I}' & 0\end{pmatrix}\begin{pmatrix}\delta_{\widehat{v}}H\\ \delta_{\overline{\widehat{v}}}H\end{pmatrix}, \end{aligned}$$

therefore Eq. (41) for $\widehat{v}$ is also Hamiltonian with the same symplectic structure (30) as for u and $\widehat{u}$. That (40) is a canonical transformation should be expected since all the linear terms in (38) have counterparts in the corresponding Hamiltonian (39), and thus (40) can be thought of as a phase change (in Fourier space) which further renormalizes the Hamiltonian by subtracting off the linear contributions.

We integrate (41) in time using a symplectic fourth-order (2-stage) Gauss–Legendre Runge–Kutta scheme [26],

$$\begin{aligned} \widehat{v}^{n+1} &= \widehat{v}_n + \Delta\tau[b_1\widetilde{\mathcal{N}}(\widehat{v}^{(1)}) + b_2\widetilde{\mathcal{N}}(\widehat{v}^{(2)})], \\ \widehat{v}^{(1)} &= \widehat{v}_n + \Delta\tau[a_{11}\widetilde{\mathcal{N}}(\widehat{v}^{(1)}) + a_{12}\widetilde{\mathcal{N}}(\widehat{v}^{(2)})], \\ \widehat{v}^{(2)} &= \widehat{v}_n + \Delta\tau[a_{21}\widetilde{\mathcal{N}}(\widehat{v}^{(1)}) + a_{22}\widetilde{\mathcal{N}}(\widehat{v}^{(2)})], \end{aligned} \tag{42}$$

for the solution $\widehat{v}^{n+1}$ at $\tau_{n+1} = \tau_n + \Delta\tau$, where $\Delta\tau$ is the constant time step and

$$\begin{aligned} &a_{11} = a_{22} = \frac{1}{4}, \qquad a_{12} = \frac{1}{4} + \frac{\sqrt{3}}{6}, \qquad a_{21} = \frac{1}{4} - \frac{\sqrt{3}}{6}, \\ &b_1 = b_2 = \frac{1}{2}, \qquad c_1 = \frac{1}{2} + \frac{\sqrt{3}}{6}, \qquad c_2 = \frac{1}{2} - \frac{\sqrt{3}}{6}. \end{aligned}$$

By inverting (40), we can rewrite (42) in terms of $\widehat{u}$ as

$$\begin{aligned} \widehat{u}^{n+1} = & \ e^{\mathcal{L}\Delta\tau}\widehat{u}^n + \Delta\tau e^{\mathcal{L}\Delta\tau}[b_1 e^{-c_1\mathcal{L}\Delta\tau}\mathcal{N}(e^{c_1\mathcal{L}\Delta\tau}\widehat{u}^{(1)}) \\ & + b_2 e^{-c_2\mathcal{L}\Delta\tau}\mathcal{N}(e^{c_2\mathcal{L}\Delta\tau}\widehat{u}^{(2)})], \end{aligned} \tag{43}$$

$$\begin{aligned} \widehat{u}^{(1)} = & \ \widehat{u}^n + \Delta\tau a_{11}e^{-c_1\mathcal{L}\Delta\tau}\mathcal{N}(e^{c_1\mathcal{L}\Delta\tau}\widehat{u}^{(1)}) \\ & + \Delta\tau a_{12}e^{-c_2\mathcal{L}\Delta\tau}\mathcal{N}(e^{c_2\mathcal{L}\Delta\tau}\widehat{u}^{(2)}), \end{aligned} \tag{44}$$

$$\begin{aligned} \widehat{u}^{(2)} = & \ \widehat{u}^n + \Delta\tau a_{21}e^{-c_1\mathcal{L}\Delta\tau}\mathcal{N}(e^{c_1\mathcal{L}\Delta\tau}\widehat{u}^{(1)}) \\ & + \Delta\tau a_{22}e^{-c_2\mathcal{L}\Delta\tau}\mathcal{N}(e^{c_2\mathcal{L}\Delta\tau}\widehat{u}^{(2)}). \end{aligned} \tag{45}$$

At each time step, the values of $\widehat{u}^{(1)}$ and $\widehat{u}^{(2)}$ required in (43) to update $\widehat{u}^{n+1}$ are obtained by solving the nonlinear system

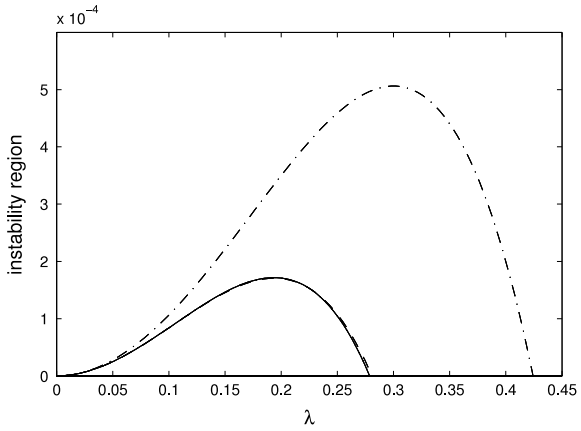

Fig. 2. Comparison of instability regions for $A_0 = 0.15$, $\varepsilon = 1$ and $\mu = 0$ $(n = 2)$ between the NLS equation (dotted-dashed line), the Hamiltonian Dysthe equation (dashed line), model (36) (dotted line) and model (38) (solid line). The instability curves for the latter two models are given by conditions (34) and (35).

(44)–(45). This is accomplished through fixed point iteration with the initial guess for $\widehat{u}^{(1)}$ and $\widehat{u}^{(2)}$ given by the solution $\widehat{u}^n$ at time τ_n. A similar scheme was used in [13] to solve the full Eqs. (6)–(7). For all the applications shown in the present paper, three iterations were typically needed to solve the nonlinear system given a convergence tolerance of 10^{-8} on the relative error. This was found to be a good compromise between accuracy and computational cost.

We point out that the numerical methods for space discretization and time integration, as described above, can be readily extended to the three-dimensional case $(n = 3)$.

8.2. Discussion of results

For our two-dimensional simulations, we non-dimensionalize the equations according to Stokes wave theory in deep water by multiplying lengths by k_0 and multiplying times by $\omega(k_0)$ so that both $g = 1$ and $k_0 = 1$. Having the test on Benjamin–Feir instability in mind, we start our computations with the perturbed solution

$$u(X, 0) = A_0[1 + a_p \cos(\lambda_p X)].$$

Since the main goal of this section is to illustrate properties of models (36) and (38) along with the performance of the symplectic time integrator, we will restrict our attention to the case $A_0 = 0.15$, $\varepsilon = 1$, $a_p = 0.01$ and $\lambda_p = 0.2$. Because of our choice of non-dimensionalization, specifying $A_0 \ll 1$ while fixing $\varepsilon = 1$ is equivalent to specifying $\varepsilon \ll 1$ while fixing $A_0 = 1$. The initial wave steepness is measured by the parameter A_0.

We have typically observed that smaller values of A_0 and a_p induce slower evolutions in time (and thus longer computations), while larger values induce faster evolutions, quickly leading to higher-frequency physical/numerical instabilities beyond the Benjamin–Feir regime due to the higher nonlinearities involved. Therefore, the choice of $A_0 = 0.15$ (and $a_p = 0.01$) was found to be a good compromise for the purpose of our numerical illustrations. The value $\lambda_p = 0.2$ corresponds to the most unstable disturbance as shown in Fig. 2. For comparison again, we also plot the instability curves for the NLS and Hamiltonian Dysthe equations. Note that the curves for (36) and (38) are indistinguishable at the graphical scale of Fig. 2.

Figs. 3 and 4 show the time evolution of the relative errors on M and H up to $\tau = 2500$, where M_0 and H_0 are the initial values at $\tau = 0$. We used a computational domain of length $L = 20\pi$ with spatial resolution $N = 256$ and time step $\Delta\tau = 10^{-3}$. The value of $\Delta\tau$ is selected such that it is much smaller than the smallest linear period allowed by the chosen spatial resolution. Overall, both M and H are very well conserved by the two models, although the corresponding errors exhibit a tendency to grow in time. This growth is likely due to the accumulation of numerical errors, which is aggravated by the development of the Benjamin–Feir instability, and is more pronounced for model (38), especially with regards to the conservation of H.

Fig. 5 depicts the time evolution of the normalized amplitudes for the fundamental and sideband harmonics, $|\widehat{u}(0)|$ and $|\widehat{u}(\pm\lambda_p)|$.

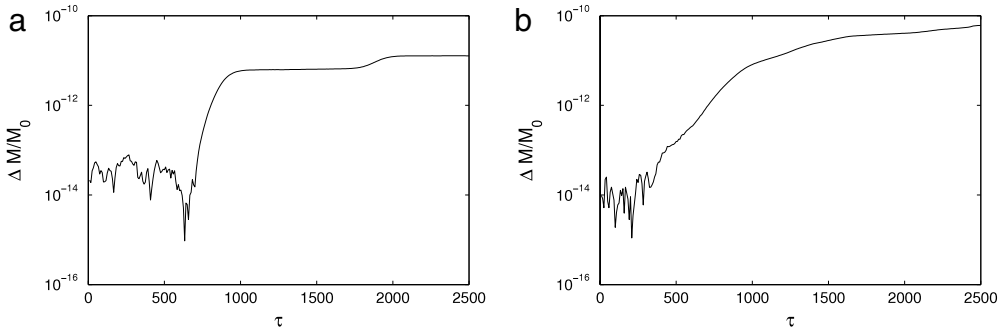

Fig. 3. Relative error on wave action M as a function of time for $A_0 = 0.15$, $\varepsilon = 1$, $a_p = 0.01$ and $\lambda_p = 0.2$. Left panel: model (36). Right panel: model (38).

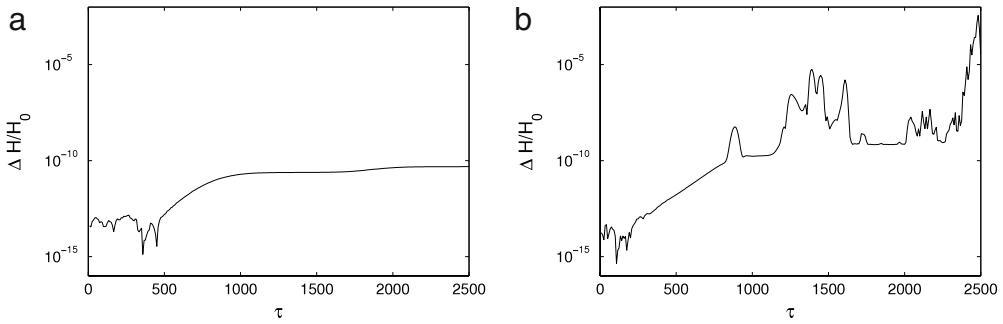

Fig. 4. Relative error on Hamiltonian H as a function of time for $A_0 = 0.15$, $\varepsilon = 1$, $a_p = 0.01$ and $\lambda_p = 0.2$. Left panel: model (36). Right panel: model (38).

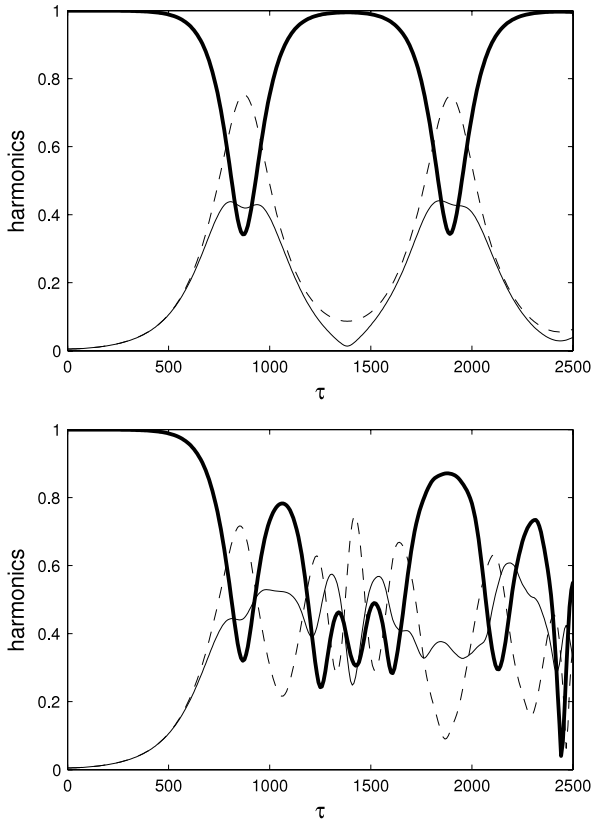

Fig. 5. Normalized harmonics as a function of time for $A_0 = 0.15$, $\varepsilon = 1$, $a_p = 0.01$ and $\lambda_p = 0.2$. Fundamental $|\widehat{u}(0)|$ (thick solid line). Lower sideband $|\widehat{u}(-\lambda_p)|$ (dashed line). Upper sideband $|\widehat{u}(\lambda_p)|$ (thin solid line). Top panel: model (36). Bottom panel: model (38).

For model (36), the near-recurring exchange of energy between the fundamental and sidebands is consistent with previous observations of the Benjamin–Feir instability for waves of relatively small amplitude and bandwidth (e.g. [24,27,1,13]). The asymmetric evolution of the two sidebands, with the lower sideband being more excited than the upper one, is also a well-known feature of the phenomenon. It is mainly due to the higher-order nonlinear term $|u|^2\partial_X u$ in the equations, which has a skewness effect on both the physical and spectral aspects of the solution. In contrast, the results for model (38) show a more irregular pattern, which may be explained by the fact that the exact linear dispersion combined with the moderately small wave steepness allows the Benjamin–Feir instability to cause sufficient wave modulations to trigger higher-wavenumber instabilities. This superposition of instabilities could then result in the observed irregular behavior.

Finally, Figs. 6 and 7 show snapshots of the envelope magnitude $|u|$ together with the corresponding (rescaled) free-surface elevation $\varepsilon^{-1}\eta$. The latter can be determined from the envelope u using the transformation (11) and, in the present numerical setting, it can be easily computed as

$$\eta(X,\tau) = \frac{\varepsilon}{\sqrt{2}}\left[\mathcal{F}^{-1}\left(\sqrt[4]{\frac{|k_0+\varepsilon^{1/2}\lambda|}{g}}\,\widehat{u}\right)e^{ik_0X/\sqrt{\varepsilon}} + \text{c.c.}\right]. \quad (46)$$

This expression neglects the mean field $\widetilde{\eta}$ which does not contribute at the order of approximation considered here, but it exactly accounts for all the contributions from the higher sideband harmonics since it includes the exact expression of G_0. Overall, for both models (36) and (38), the solution develops strong amplitude modulations as a result of the Benjamin–Feir instability. We clearly see the development of the left–right asymmetry in the profile of

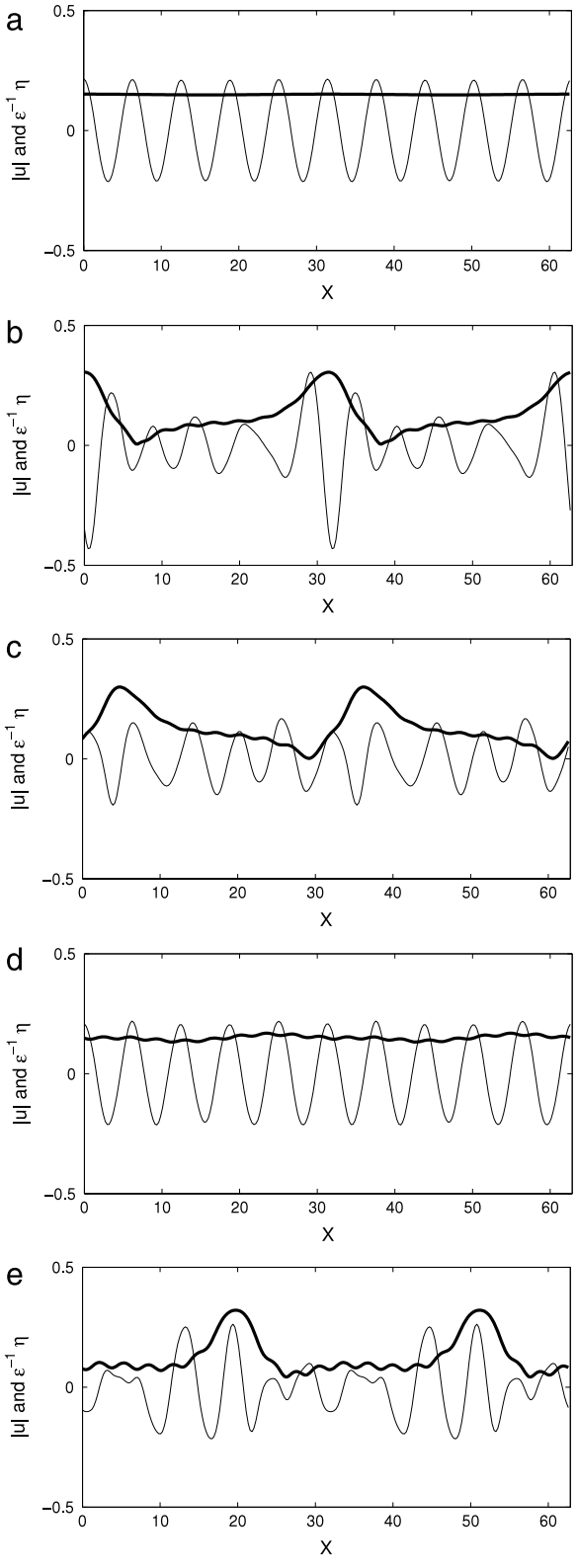

Fig. 6. Snapshots of the envelope magnitude $|u|$ (thick solid line) and free-surface elevation $\varepsilon^{-1}\eta$ (thin solid line) for model (36) at (a) $\tau = 0$, (b) 799.967, (c) 949.961, (d) 1366.611 and (e) 1866.591, for $A_0 = 0.15$, $\varepsilon = 1$, $a_p = 0.01$ and $\lambda_p = 0.2$.

$|u|$, especially at the initial stages of the wave evolution, which is related to the skewness effect as discussed earlier. The more unstable behavior for (38) as shown in Fig. 7 is in accordance with our previous observation from Fig. 5, and suggests that higher-wavenumber instabilities also come into play. We note

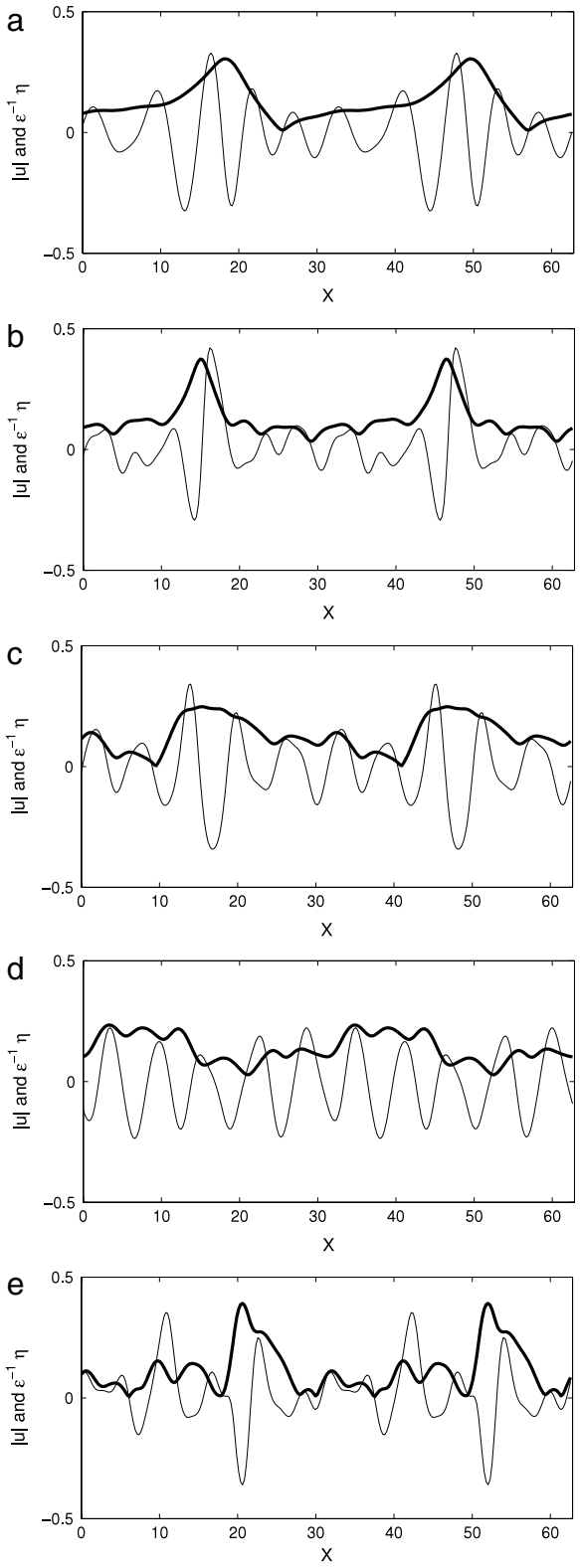

Fig. 7. Snapshots of the envelope magnitude $|u|$ (thick solid line) and free-surface elevation $\varepsilon^{-1}\eta$ (thin solid line) for model (38) at (a) $\tau = 791.634$, (b) 1399.943, (c) 1766.595, (d) 1924.922 and (e) 2500, for $A_0 = 0.15$, $\varepsilon = 1$, $a_p = 0.01$ and $\lambda_p = 0.2$.

interestingly that the profile of $|u|$ does not exactly coincide with the actual shape of the free-surface envelope everywhere at every instant, although there is some correlation in the position of their respective maximum amplitudes. This difference may be explained in part by the fact that the relation (11) between u and η is not a simple relation of proportionality due to the presence of the Fourier multiplier $a^{-1}(D_x)$, and therefore one should be careful about the physical interpretation of u. In contrast, the dependent variable in the original models of Trulsen and Dysthe [4] and Trulsen et al. [5] is more closely related to the free-surface envelope.

Finally we point out that, for a more correct reconstruction of the free-surface elevation from e.g. (36), the inverse Fourier transform $\mathcal{F}^{-1}$ in (46) should be translated by

$$X \to X - \partial_k\omega(k_0)\tau/\sqrt{\varepsilon},$$

and multiplied by the additional phase factor

$$e^{-i[\omega(k_0)-k_0\partial_k\omega(k_0)]\tau/\varepsilon},$$

which is related to the subtractions of M and I from H as discussed in Section 5. Similar considerations apply to model (38). These adjustments however have no major effect on the results shown in Figs. 6 and 7.

9. Conclusions

We have applied the Hamiltonian approach of Craig et al. [8,9] to deriving Hamiltonian versions of the higher-order NLS models for broader-banded deep-water waves, originally proposed by Trulsen and Dysthe [4] and Trulsen et al. [5]. The Benjamin–Feir instability regions for these new models were then determined, and a good agreement was found in comparison with previous work. Finally, numerical simulations were shown to illustrate these stability results and check the conservative properties of our models. With this aim, we have introduced an efficient and accurate symplectic scheme for time integration, combined with a pseudospectral method for space discretization.

Acknowledgments

W.C. is partially supported by the Canada Research Chairs Program and NSERC through grant No. 238452-06. P.G. is partially supported by the National Science Foundation through grant No. DMS-0920850. C.S. is partially supported by NSERC through grant No. 46179-05.

References

[1] D.U. Martin, H.C. Yuen, Quasi-recurring energy leakage in the two-space-dimensional nonlinear Schrödinger equation, Phys. Fluids 23 (1980) 881–883.
[2] K.B. Dysthe, Note on a modification to the nonlinear Schrödinger equation for application to deep water waves, Proc. R. Soc. Lond. A 369 (1979) 105–114.
[3] U. Brinch-Nielsen, I.G. Jonsson, Fourth order evolution equations and stability analysis for Stokes waves on arbitrary water depth, Wave Motion 8 (1986) 455–472.
[4] K. Trulsen, K.B. Dysthe, A modified nonlinear Schrödinger equation for broader bandwidth gravity waves on deep water, Wave Motion 24 (1996) 281–289.
[5] K. Trulsen, I. Kliakhandler, K.B. Dysthe, M.G. Velarde, On weakly nonlinear modulation of waves on deep water, Phys. Fluids 12 (2000) 2432–2437.
[6] J.W. McLean, Instabilities of finite-amplitude water waves, J. Fluid Mech. 114 (1982) 315–330.
[7] V.E. Zakharov, Stability of periodic waves of finite amplitude on the surface of a deep fluid, J. Appl. Mech. Tech. Phys. 9 (1968) 190–194.
[8] W. Craig, P. Guyenne, C. Sulem, A Hamiltonian approach to nonlinear modulation of surface water waves, Wave Motion 47 (2010) 552–563.
[9] W. Craig, P. Guyenne, C. Sulem, Coupling between internal and surface waves, Nat. Hazards 57 (2011) 617–642.
[10] O. Gramstad, K. Trulsen, Hamiltonian form of the modified nonlinear Schrödinger equation for gravity waves on arbitrary depth, J. Fluid Mech. 670 (2011) 404–426.
[11] V.P. Krasitskii, On reduced equations in the Hamiltonian theory of weakly nonlinear surface waves, J. Fluid Mech. 272 (1994) 1–20.
[12] W. Craig, C. Sulem, Numerical simulation of gravity waves, J. Comput. Phys. 108 (1993) 73–83.
[13] L. Xu, P. Guyenne, Numerical simulation of three-dimensional nonlinear water waves, J. Comput. Phys. 228 (2009) 8446–8466.
[14] R. Coifman, Y. Meyer, Nonlinear harmonic analysis and analytic dependence, Proc. Sympos. Pure Math. 43 (1985) 71–78.
[15] O.M. Phillips, On the dynamics of unsteady gravity waves of finite amplitude. Part 1. The elementary interactions, J. Fluid Mech. 9 (1960) 193–217.

[16] A. de Bouard, W. Craig, O. Díaz-Espinosa, P. Guyenne, C. Sulem, Long wave expansions for water waves over random topography, Nonlinearity 21 (2008) 2143–2178.
[17] W. Craig, M.D. Groves, Hamiltonian long-wave approximation to the water-wave problem, Wave Motion 19 (1994) 367–389.
[18] W. Craig, P. Guyenne, J. Hammack, D. Henderson, C. Sulem, Solitary water wave interactions, Phys. Fluids 18 (2006) 057106.
[19] W. Craig, P. Guyenne, D.P. Nicholls, C. Sulem, Hamiltonian long-wave expansions for water waves over a rough bottom, Proc. R. Soc. Lond. A 461 (2005) 839–873.
[20] W. Craig, P. Guyenne, C. Sulem, Water waves over a random bottom, J. Fluid Mech. 640 (2009) 79–107.
[21] P. Guyenne, D.P. Nicholls, A high-order spectral method for nonlinear water waves over moving bottom topography, SIAM J. Sci. Comput. 30 (2007) 81–101.
[22] W. Craig, P. Guyenne, H. Kalisch, Hamiltonian long-wave expansions for free surfaces and interfaces, Commun. Pure Appl. Math. 58 (2005) 1587–1641.
[23] W. Craig, C. Sulem, P.-L. Sulem, Nonlinear modulation of gravity waves: a rigorous approach, Nonlinearity 5 (1992) 497–522.
[24] S. Leblanc, Stability of bichromatic gravity waves on deep water, Eur. J. Mech. B/Fluids 28 (2009) 605–612.
[25] P.A. Milewski, E.G. Tabak, A pseudospectral procedure for the solution of nonlinear wave equations with examples from free-surface flows, SIAM J. Sci. Comput. 21 (1999) 1102–1114.
[26] B. Leimkuhler, S. Reich, Simulating Hamiltonian Dynamics, Cambridge University Press, Cambridge, 2004.
[27] M.S. Longuet-Higgins, The instabilities of gravity waves of finite amplitude in deep water II. Subharmonics, Proc. R. Soc. Lond. A 360 (1978) 489–505.